










Elucidating the Effect of the Different Buffer Layers on the Thermal Stability of CIGSe Solar Cells

Hasan A. Yetkin , Tim Kodalle , Tobias Bertram, Alejandra Villanueva Tovar , Reiner Klenk , Marin Rusu , Josefa Ibaceta-Jaña, Florian Ruske , Ibrahim Simsek , Ruslan Muydinov, Bernd Szyszka, Rutger Schlatmann , and Christian A. Kaufmann 

Abstract—In this contribution, the impact of thermal stress on Cu(In,Ga)Se₂ (CIGSe) thin film photovoltaic devices is investigated. The tolerance of such devices to high temperatures is of particular interest for processing transparent conductive oxides (TCOs) in order to further close the gap to the theoretical efficiency limit and for their potential use as bottom devices in tandem applications in order to overcome the theoretical efficiency limit of single junction solar cells. When CdS-buffered CIGSe high efficiency solar cells are subjected to thermal stress, elemental interdiffusion of Na and Cd between the absorber and the window layers as well as chemical reactions at the CIGSe/CdS interface result in a degraded power conversion efficiency (PCE). Here, we compare the degradation mechanisms of CdS and GaO_x buffered CIGSe solar cells under thermal stress. A model explaining the observed degradation behaviors is proposed.

Index Terms—Amorphous buffer layer, Cu(In,Ga)Se₂ (CIGSe) solar cells, CdS, thermal stability, GaO_x.

I. INTRODUCTION

Cu(In,Ga)Se₂ (CIGSe) thin film solar cells have attracted the attention of science and industry by attaining a maximum

Manuscript received December 8, 2020; revised January 16, 2021; accepted January 19, 2021. Date of publication February 9, 2021; date of current version April 21, 2021. This work was supported in part by the Ministry of National Education of the Republic of Turkey, Scholarship Becas Chile-DAAD 2017/91645541, and in part by the German Federal Ministry for Economic Affairs, and Energy (BMWi) under Contract 0324095H (speedCIGS). (*Corresponding author: Hasan A. Yetkin.*)

Hasan A. Yetkin and Alejandra Villanueva Tovar are with the Helmholtz-Zentrum Berlin für Materialien und Energie, 12489 Berlin, Germany, and also with the Technical University Berlin, 10587 Berlin, Germany (e-mail: hasan.yetkin@helmholtz-berlin.de; alejandra.villanueva_tovar@helmholtz-berlin.de).

Tim Kodalle, Tobias Bertram, Reiner Klenk, Marin Rusu, Florian Ruske, Ibrahim Simsek, and Christian A. Kaufmann are with Helmholtz-Zentrum Berlin für Materialien und Energie, 12489 Berlin, Germany (e-mail: tim.kodalle@helmholtz-berlin.de; tobias.bertram@helmholtz-berlin.de; klenk@helmholtz-berlin.de; rusu@helmholtz-berlin.de; florian.ruske@helmholtz-berlin.de; ibrahim.simsek@helmholtz-berlin.de; kaufmann@helmholtz-berlin.de).

Josefa Ibaceta-Jaña, Ruslan Muydinov, and Bernd Szyszka are with the Technical University Berlin, 10587 Berlin, Germany (e-mail: ibacetajana@campus.tu-berlin.de; ruslan.muydinov@tu-berlin.de; bernd.szyszka@tu-berlin.de).

Rutger Schlatmann is with Helmholtz-Zentrum Berlin für Materialien und Energie, 12489 Berlin, Germany, and also with Hochschule für Technik und Wirtschaft Berlin, 12459 Berlin, Germany (e-mail: rutger.schlatmann@helmholtz-berlin.de).

Color versions of one or more figures in this article are available at <https://doi.org/10.1109/JPHOTOV.2021.3053483>.

Digital Object Identifier 10.1109/JPHOTOV.2021.3053483

efficiency of 23.35% which is one of the highest PCE among all polycrystalline thin film solar cells [1]. In order to surpass the theoretical limit of about 33% for single junction solar cells at a bandgap energy of 1.15 eV [2], research regarding tandem solar cells is intensified, where CIGSe can be used as a bottom device. Using such tandem solar cells, the theoretical limit for the PCE is increased to up to 46% [3]. An efficiency of 24.2% for a Perovskite/CIGSe tandem device has already been demonstrated in a two terminal structure [4]. In order to be able to further close the gap to the theoretical efficiency limit, the thermal stability of CIGSe solar cells for the use of bottom devices in tandem applications is of importance, as this will increase the process window—in terms of deposition temperature—for efficient top device components. Thermally stable CIGSe solar cells would also enable to increase the options for future attractive top devices in tandem devices, including transparent conductive oxides (TCOs).

When high efficiency CIGSe solar cells are exposed to thermal stress, chemical reactions at the *pn*-junction and elemental interdiffusion of Cu, Na, and Cd between absorber and window layer were shown to be critical issues [5]–[7]. In order to replace the CdS buffer layer with a possibly thermally stable alternative, certain criteria have to be fulfilled [8].

- 1) A correct band alignment of the conduction band minimum (CBM) between the *p*-type CIGSe absorber and the *n*-type buffer layer. The electron affinity of a buffer layer should be 0.1–0.3 eV lower than that of the CIGSe absorber layer depending on the Ga-gradient on the CIGSe surface in order to limit interface recombination.
- 2) An *n*-type doping in the order of 10¹⁸ cm⁻³ of the buffer layer in order to achieve sufficient type-inversion within the CIGSe absorber surface.
- 3) A large optical bandgap of the buffer material to minimize the parasitic absorption loss.
- 4) An amorphous morphology and high chemical stability of the ideal buffer to prevent elemental interdiffusion between absorber and window layer as well as chemical reactions.

Amorphous thin films can potentially suppress the elemental interdiffusion between the respective layers due to the absence of grain boundaries.

In the light of the abovementioned criteria, amorphous GaO_x emerges as a good candidate, showing high chemical stability and comparable electron affinity to that of CIGSe or at least

facilitating the electron transport over subgap defects due to oxygen deficiency in the layer [8]–[11]. In this contribution, we compare the thermal stability of CdS-buffered and GaO_x-buffered CIGSe solar cells and discuss their respective degradation mechanisms using various analytical techniques.

Please note that this study as “enhanced manuscript” is the continuation of the work we recently presented at the IEEE Photovoltaic Specialist Conference [12]. In the present study, the discussion of the degradation mechanism of the CdS- and GaO_x-buffered CIGSe solar cells is extended and supported by conducting additional experiments in order to better understand the effects of Na presence and annealing environment on the degradation mechanisms. Temperature-dependent current-voltage (*JV-T*) measurements are also performed on the GaO_x-buffered CIGSe solar cells before and after thermal stress. Furthermore, optical and structural properties of the sputter deposited GaO_x thin films are shown. Finally, Raman spectroscopy measurements on GaO_x thin films are carried out to examine their structures in detail.

II. METHODS

Using a three-stage thermal coevaporation process, $\sim 2.15\text{-}\mu\text{m}$ thick CIGSe thin films with a nominal [Cu]/([In]+[Ga])-ratio (CGI) of 0.9 and a nominal [Ga]/([In]+[Ga])-ratio (GGI) of 0.3 are coevaporated at a nominal deposition temperature of 530°C on 800-nm Mo/2-mm soda–lime glass (Na incorporation from glass through Mo) or Mo/SiO_xN_y/2-mm soda–lime glass (no Na incorporation into CIGSe absorber). It is worth to note that no additional alkali post deposition treatment has been carried out for the devices investigated in this study. Further details of the adapted three-stage process can be found in [13]. In total there are four nominally identical absorber processes, two with Na and two without Na. For each absorber process one CdS reference “as deposited” device was prepared. After washing of the CIGSe layer with 10% NH₃ (aq) for 2 min, devices were individually completed by either a chemical bath deposited CdS buffer layer or a GaO_x buffer layer with a nominal thickness of 60 nm, deposited at room temperature via radio frequency (rf) sputtering. Sputtering processes for GaO_x deposition were conducted under pure argon (Ar) atmosphere with a background pressure of 5 μbar and with a sputtering power density of 0.54 Wcm^{-2} . Note that prior to GaO_x buffer layer deposition, bare absorber layers without Na (prepared on glass substrates with Na-diffusion barrier) were air-annealed at 300°C for 20 min in order to enhance overall device efficiency as demonstrated in [7]. Directly after depositing the GaO_x layer, the sample was postannealed at 150°C for 20 min without vacuum break in order to achieve optimum device performance. Finally, a sputtered bi-layer consisting of a 40-nm thick intrinsic ZnO (i-ZnO) and a 150-nm thick doped ZnO:Al (AZO) as well as an e-beam evaporated Ni/Al/Ni contact grid were deposited.

In order to investigate the behavior after thermal stress, the CdS- and GaO_x-buffered solar cells each were exposed to annealing in air and under vacuum at 300°C for 20 min directly after the ZnO-bilayer deposition. For air-annealing a simple hot plate was used inside a flowbox and for vacuum-annealing a

radiation heater (located below the sample) has been employed inside a vacuum chamber ($\sim 10^{-7}$ mbar). Both systems were preheated to the desired temperature of 300°C prior to the annealing. After temperature stabilization, the respective samples were exposed to thermal annealing. The lateral temperature error for air-annealing was determined by measuring the surface temperature of the hot plate with a temperature sensor and for vacuum-annealing temperature stickers (ATP Messtechnik) were attached to the back side of the sample. Accordingly, a deviation of $\Delta T = \pm 2^\circ\text{C}$ for hot plate and a deviation of $\Delta T = \pm 5^\circ\text{C}$ for vacuum-annealing have been determined. Thus, an annealing temperature of 300°C was ensured in both systems. For the respective annealing treatments, only samples from the same absorber process have been used in order to ensure comparability. For instance, for air- and vacuum-annealing of the CdS buffered devices with Na, all samples are from the same CIGSe deposition process with the CdS reference indicating the overall quality of the absorbers from that process. Quantified glow discharge optical emission spectrometry (GD-OES) measurements (such as those shown in Fig. 4) have shown that the Na-content of Na-free samples is < 1 ppm, while that of Na-containing samples is > 50 ppm. We therefore believe to be able to rule out any cross contamination between processes, even though these processes have been performed in the same deposition tool.

Solar cell performances were measured under standard test conditions (AM 1.5 G, 1000 Wm^{-2} , 25°C) using a WACOM A+ solar simulator. Temperature dependent current-voltage (*JV-T*) measurements were conducted under vacuum and in a liquid N₂ cooled cryostat (CryoVac) using a Keithley 2601 A source measurement unit in four-point contact configuration and an LED solar simulator (Oriel VeraSol) imitating an AM1.5 G solar spectrum with a light intensity of 1000 Wm^{-2} . The temperature ranges from 320 up to 90 K with a step size of 10 K. Capacitance–voltage (*CV*) measurements were carried out in the dark using a custom built setup. Sheet resistance measurements by four-point probe were done on the AZO layers on top of the CIGSe solar cell stack. GD-OES using a Spectrumba GDA 650 tool was applied to the samples in order to determine elemental in-depth profiles following the procedure described in [14]. The quantification of the GD-OES profiles was only possible for the CdS-buffered CIGSe devices, not for the GaO_x-buffered CIGSe devices, since a calibration sample for GaO_x was not available. Please note that the Na depth profiles were smoothed in order to ease visibility.

Total transmission and total reflection have been measured on samples that were grown directly on quartz substrates using the Lambda 1050 Spectrophotometer by Perkin Elmer in order to explore the optical properties of the GaO_x such as band gap (E_g). Spectroscopic ellipsometry has been performed on the same sample. The results from UV–Vis and spectroscopic ellipsometry measurements were fitted via Rig-VM to obtain a close model of the optical parameters [15]. We employed temperature-dependent X-Ray diffraction (XRD) analyses in grazing incidence (GI-XRD) and Bragg Brentano (BB-XRD) geometries to disclose the crystallization route of GaO_x layers in the temperature range from 600 up to 800°C and from 450 up to 1000°C under vacuum conditions, respectively. The D8 Discovery XRD system from AXS Bruker (Germany) with Cu K α

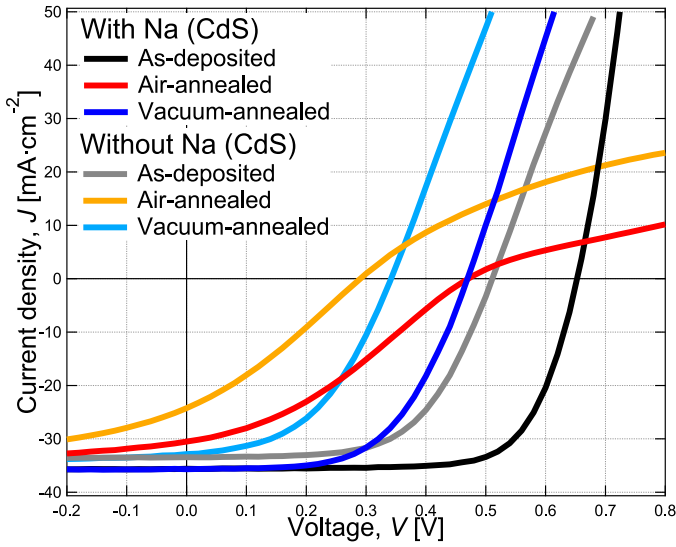


Fig. 1. JV -curves of the measured CdS-buffered CIGSe solar cells with and without Na before and after thermal stress at 300°C for 20 min in air and under vacuum.

radiation was used. Samples were heated under vacuum ($\sim 10^{-5}$ mbar) in a Be-dome module from Anton Paar (Austria). For the GI-XRD measurements a Göbel mirror in combination with equatorial soller (0.25°) was used and the sample surface was preset to be parallel to the straight beamline. Micro-Raman spectroscopy has been conducted in order to further investigate the structural properties of the GaO_x layers using a high-resolution LabRAM HR800 spectrometer from Horiba with the excitation wavelength of 532 nm and a power magnitude of 20.6 mW.

III. RESULTS AND DISCUSSION

A. CdS-Buffered Devices

Fig. 1 shows the effect of the annealing environment and incorporation of Na on the JV -characteristics of the CdS-buffered CIGSe solar cells. At first glance, the positive effect of Na incorporation on the device power conversion efficiencies can be seen from the comparison of the as-deposited solar cells with and without Na. Vacuum-annealing of the devices with Na leads to a strong decrease in V_{OC} with a slight distortion in the JV -curve, while air-annealing results in a V_{OC} reduction of the same magnitude. However, air-annealing leads to additional adverse effects in J_{SC} and in the shape of the JV -curve, that indicates a strong roll-over and kink anomaly [16]. The devices without Na also show severe degradations in PV-parameters, which are most pronounced after air-annealing with a decrease in J_{SC} and kink as well as roll-over anomaly. Table I shows the PV-parameters of the devices before and after annealing. All in all the electrical degradation of the CIGSe solar cell devices with and without Na are primarily independent of the annealing environment. Moreover, air-annealing brings about further degeneration of J_{SC} and fill factor (FF) as well as occurrence of the anomalies in the JV -curves.

Comparing the charge carrier concentration (N_{CV}) of the as-deposited devices with and without Na in Fig. 2 highlights the

TABLE I
PV-PARAMETERS FOR CdS-BUFFERED SOLAR CELLS BEFORE AND AFTER THERMAL ANNEALING

	V_{OC} (mV)	J_{SC} (mA/cm ²)	FF (%)	η (%)
As-depo w Na	652	35.6	72.5	16.8
VA w Na	469	35.7	57.4	9.6
AA w Na	471	30.5	33.8	4.9
As-depo w/o Na	511	33.4	60.4	10.3
VA w/o Na	342	32.8	47.3	5.3
AA w/o Na	290	24.3	29.5	2.1

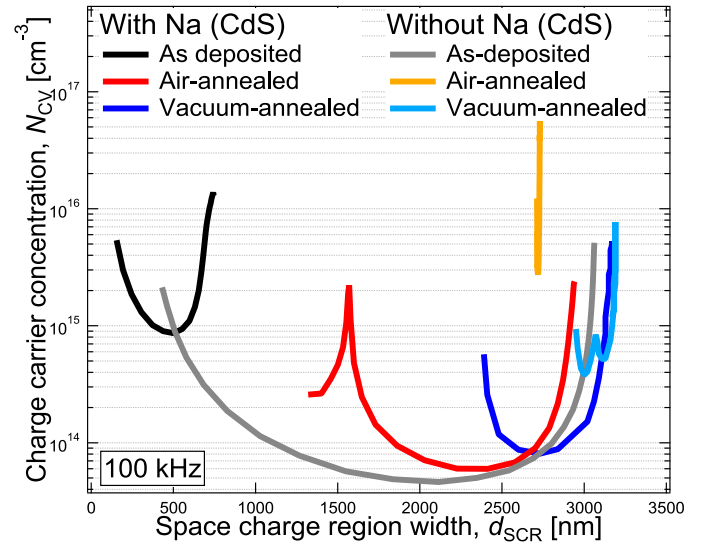


Fig. 2. N_{CV} -profiles of the CdS-buffered CIGSe solar cells with and without Na before and after thermal stress.

beneficial effect of Na-presence in the CIGSe absorber, which is exhibited by a one order of magnitude higher N_{CV} for the device with Na. The shift of the N_{CV} -profiles toward larger width of space charge region (d_{SCR}) is observed after annealing regardless of the Na content and annealing atmosphere. Such shift of the N_{CV} -profile might be a sign of an increased barrier height at the back contact (Φ_{BC}), as reported in [7]. The loss in V_{OC} for the CdS-buffered devices with Na are to some extent caused by a reduction of the N_{CV} within the CIGSe absorber. However, the approximate various losses in V_{OC} are hard to quantify due to the strong dependence on the dominant recombination path [16]. JV - T -measurements were employed to further investigate this and help to determine the activation energy of the recombination current (E_a) and Φ_{BC} , as suggested by [17]. Fig. 3 shows the changes in V_{OC} over T for the as-deposited and annealed CdS-buffered devices with and without Na. The E_a of the as-deposited device pinpoints the minimum E_g extracted from external quantum efficiency (EQE, not shown), revealing that the main recombination pathway seems to be located in the bulk of the absorber layer, while the lack of Na in as-deposited devices initially gives rise to lower E_a than the E_g , signifying that this device is limited by recombination at the CIGSe/CdS interface. In addition to this, a back contact barrier with a height of 0.14 eV is visible in case of the as-deposited device with Na, whereas the as-deposited device without Na initially exhibits a higher $\Phi_{BC} = 0.20$ eV. With respect to the repercussions of

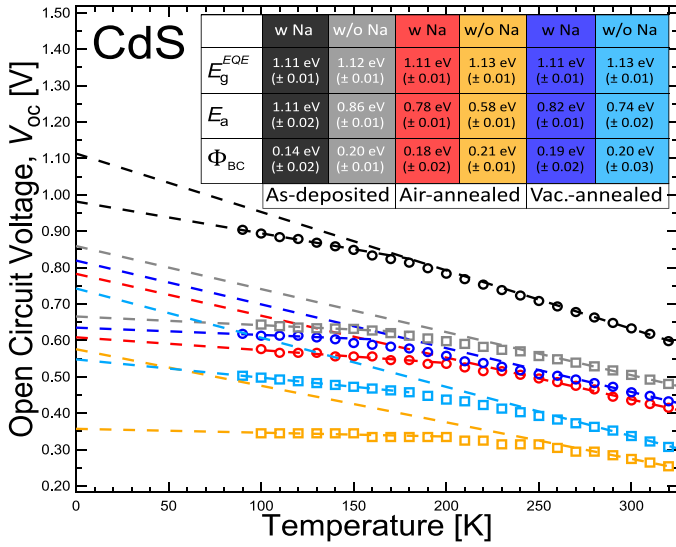


Fig. 3. V_{OC} - T characteristics under one sun illumination at temperatures from 90 to 320 K for the CdS-buffered-CIGSe solar cells with (circles) and without Na (squares).

the annealing, E_a of the devices with and without Na strongly decreases compared with the respective reference samples. This unveils that the major source of the limitation of the solar cells after annealing is due to recombination at the CIGSe/CdS interface. Beside this, the annealing seems to cause an increased Φ_{BC} in the case of devices with Na. The devices without Na, on the other hand, do not suffer from a further increasing Φ_{BC} .

The decrease in J_{SC} , which appears after thermal stress in air, can partly be attributed to an increased sheet resistance of the AZO layer of the air-annealed device with Na that indicates more than one decade higher resistivity (960 Ω /sq) than the as-deposited one (94 Ω /sq). The negative effect of Na on the AZO conductivity can be well understood by a comparison with the sheet resistance of the air-annealed device without Na, which is 420 Ω /sq. Not to mention that the vacuum-annealing does lead to slight degeneration of the conductivity in TCO layers of the devices with (113 Ω /sq) and without Na (91 Ω /sq). Consequently, the series resistance (R_s) of the air-annealed devices becomes rather high, which in part explains the decrease in J_{SC} of these devices.

Cd and Na in-depth profiles as measured by GD-OES of the as-deposited and annealed CdS devices are shown in Fig. 4(a) and (b). In order to make a reasonable comparison, the depth profiles are aligned to their respective onset of the Cd-signal. Air-annealing of the devices regardless of the Na-presence causes significant Cd-diffusion into the CIGSe absorber layer, while vacuum-annealing leads to less Cd-diffusion. It is well known that Cd in CIGSe converts the CIGSe from p -type into n -type [18], [19]. Regarding the Na-containing samples, the as-deposited sample shows a moderate amount of Na in the range of 200 ppm in the CIGSe absorber toward the CIGSe/Mo-interface, whilst annealing—regardless of the environment—induces a flattening of the Na-depth profile in the entire absorber and a diffusion of Na-atoms into the CdS layer to a higher extent for air-annealing. Interestingly, air-annealing provokes further

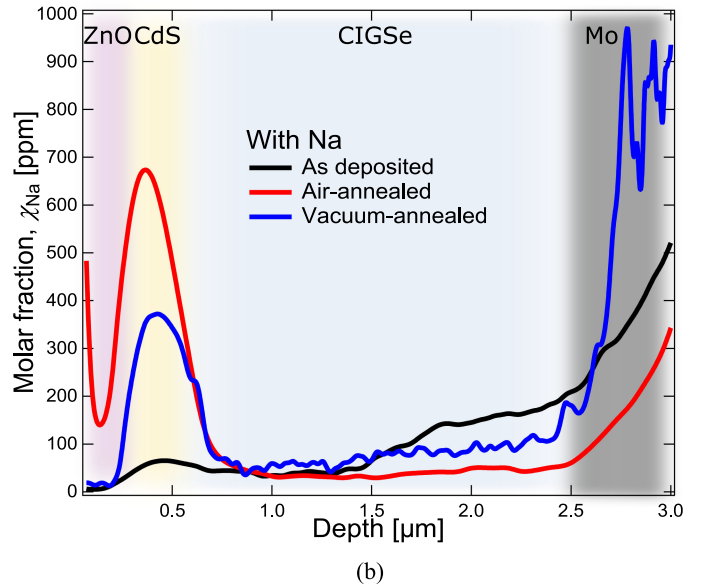
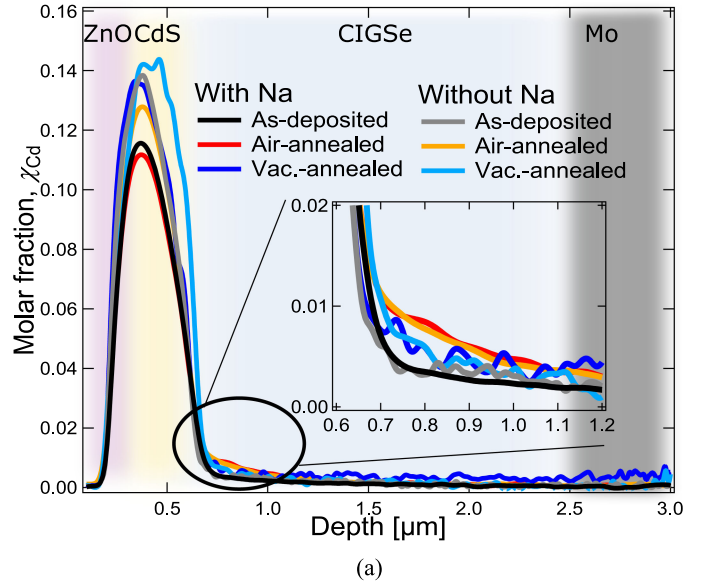


Fig. 4. (a) Cd and (b) Na in-depth profiles of as-deposited and annealed CdS-buffered devices with and without Na.

Na-diffusion toward the surface of the AZO-layer. The latter can well explain the severe increase in sheet resistance of the air-annealed device with Na as was discussed above. Another key point to bear in mind, because of the high electropositivity of the Na-ions [20], the attraction of Na into the respective front contact layers arises from water and OH^- contained in the CdS buffer layer [21] and in the ambient air. In addition, the increased back contact barrier height, that is observed for the Na-containing devices in Fig. 3, can be well corroborated by Na out-diffusion especially from the back contact area as also suggested by [7], [22], [23]. Furthermore, among other possible reasons, the appearance of the kink and roll-over anomalies might indicate deep acceptor trap states in the CdS layer [7], [24], [25] and an increased barrier height at the back contact [16], [26], [27], respectively.

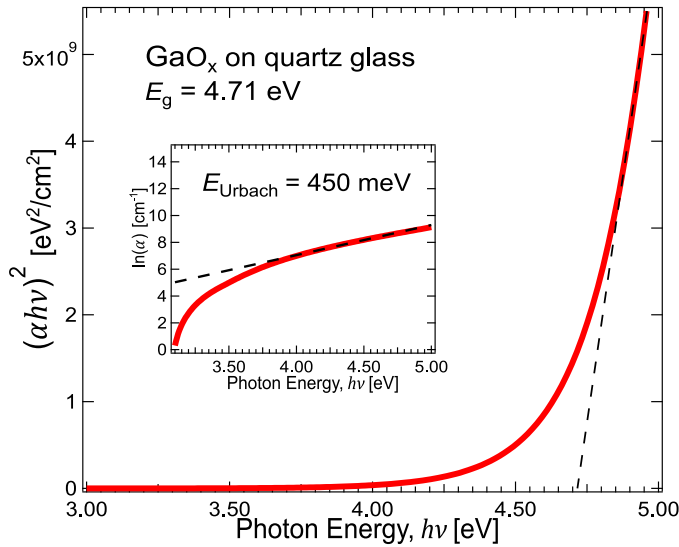


Fig. 5. Tauc plot of the GaO_x thin films deposited on quartz for optical band gap energy extracted by UV-Vis measurements. The inset shows the extracted Urbach energy of the GaO_x thin films.

Coupled with these results, the annealing induced Na out-diffusion from the CIGSe absorber into the buffer and front contact layers, when Na is present inside the CIGSe absorber paint a decisive picture of the degradations, as can be seen from the Fig. 4(b). It is important to highlight the presence of a high amount of Na within the CdS and ZnO that is also seen in Fig. 4(b). It is known from literature that Na in CdS and ZnO layers causes acceptor type defects due to its single valence electron [28]–[30]. Therefore, it is suggested here that the formation of the kink anomaly in the JV -characteristic is ascribed to the presence of acceptor trap states in the CdS layer and the increased sheet resistance of the AZO layer, that presumably provokes the additional drop in J_{SC} , is coupled with the Na presence. This effect might be amplified by the incorporation of oxygen or water from the air environment during the annealing. As will be seen below in Section C [Fig. 10(a)], Na is much less mobile within the device, if the wet nature of the buffer is eliminated, in particular if the annealing is performed in vacuum.

The strong roll-over anomaly that is observed especially for the air-annealed devices can be attributed to high Φ_{BC} values likely coupled with a stronger Cd-diffusion into the CIGSe surface, since weak Cd-diffusions into CIGSe along with similar Φ_{BC} after vacuum-annealing are evident.

The combination of all these findings reveal that the degradation of the CdS-buffered devices is independent of the annealing atmosphere for all the annealed devices, worsening of the CIGSe/CdS junction properties and back contact barrier, even though additional deteriorations occurred with air-annealing. We interpret these findings to show that the wet nature of the CdS buffer layer plays a crucial role in the degradation.

B. Optical and Structural Properties of GaO_x Thin Films

This work is focused on amorphous GaO_x , possibly a thermally more stable replacement for the CdS buffer. Fig. 5 illustrates the direct optical band gap for GaO_x deposited on

TABLE II
PV-PARAMETERS FOR GaO_x -BUFFERED SOLAR CELLS BEFORE AND AFTER THERMAL ANNEALING

	V_{OC} (mV)	J_{SC} (mA/cm ²)	FF (%)	η (%)
CdS-ref w Na	629	35.6	72.3	16.2
As-depo w Na	558	36.4	64.1	13.0
VA w Na	616	33.0	33.6	6.8
AA w Na	492	17.7	39.0	3.4
CdS-ref w/o Na	483	33.6	57.8	9.4
As-depo w/o Na	487	34.2	60.1	10.0
VA w/o Na	522	34.2	44.4	7.9
AA w/o Na	548	23.5	42.8	5.5

quartz glass. Evaluation via Tauc plot yields an E_g of 4.71 eV. Having a wide band gap energy is advantageous over CdS, as its lower band gap leads to parasitic absorption of high energy photons. The inset in Fig. 5 shows the semilogarithmic plot of the absorption coefficient over photon energy by which one can obtain the Urbach energy (E_U) from the slope of the straight line indicating the subgap defects within the band gap due to, e.g., the structural disorder [31], [32]. The calculated E_U is around 450 meV, similar to the value seen in literature [11]. We relate this to subgap defects induced by oxygen vacancies, which facilitate the transport of electrons generated in the absorber layer to the front contact. Oxygen deficiency of the GaO_x layer deposited on Si-wafer is corroborated by the EDX analysis by which O/Ga ratio of 1.22 is attained. This ratio is lower than that of stoichiometric Ga_2O_3 . The structure of the deposited GaO_x layers is investigated by temperature dependent GI-XRD (surface sensitive) and BB-XRD (bulk sensitive) as seen in Fig. 6. Initially, the GaO_x layers exhibit an amorphous structure. The GaO_x layers preserve its amorphous structure near the surface and in the bulk even after vacuum-annealing at up to 600°C, highlighting the chemical stability of the amorphous GaO_x . Above 600°C, an increasing intensity of crystalline peaks can be detected.

C. GaO_x -Buffered Devices

Finished CIGSe solar cell devices that employ GaO_x as a buffer layer show a lower V_{OC} and FF for devices with Na, as compared with the CdS reference; however, a slight gain in J_{SC} is observed, which can be attributed to the elimination of the parasitic absorption in the CdS. This gain in J_{SC} can be increased by an optimization of the ZnO-bilayer, reducing the reflectivity of the complete solar cell. Nevertheless, for the sake of comparability of samples with CdS and GaO_x , identical ZnO layers are utilized in both types of devices. All PV-parameters of the GaO_x -buffered solar cells together with the corresponding CdS reference devices are given in Table II. Significantly, in the case without Na, as-deposited GaO_x results in slightly better PV-performances than the Na-free CdS reference device. A possible reason for the lower V_{OC} and FF , in general, may be a high density of defect states at the CIGSe/ GaO_x heterointerface along with a rather low donor concentration in the GaO_x as proposed by [33], since comparable N_{CV} are observed for the as-deposited GaO_x - and CdS-buffered devices with Na in Fig. 8. However, the difference in V_{OC} for the as-deposited

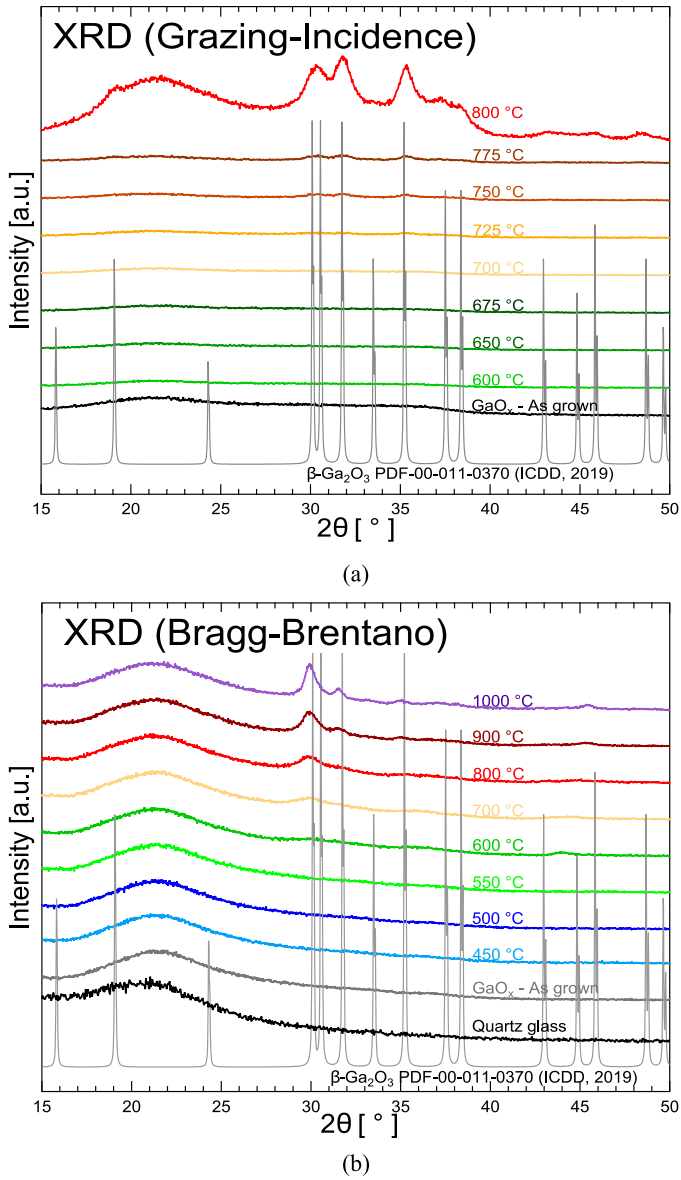


Fig. 6. Temperature dependent structural analysis of the GaO_x thin films deposited on quartz by XRD in (a) grazing-incidence and (b) Bragg-Brentano configuration.

GaO_x -buffered devices can be well explained with the difference in N_{CV} of these devices.

Regardless of the Na content, air-annealing of the GaO_x -buffered devices leads to strong decrease in J_{SC} . Moreover, a decreased V_{OC} is measured for the air-annealed device with Na despite the fact that an increased N_{CV} for both with and without Na is observed as seen in Fig. 8, while a slightly increased V_{OC} can only be seen for the air-annealed device without Na. Vacuum-annealing of the GaO_x -buffered devices shows that these devices exhibit an increased stability under thermal stress. There is no significant change in J_{SC} in both cases with and without Na, while the V_{OC} of these devices increases. The V_{OC} of the device with Na is rather high, approaching that of the CdS counterpart with Na. Vacuum-annealing of the GaO_x -buffered

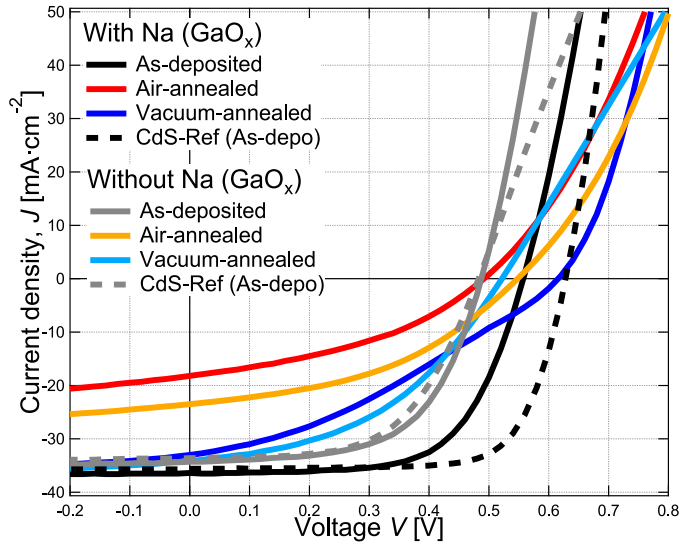


Fig. 7. JV -characteristics of the GaO_x -buffered-CIGSe solar cells with and without Na.

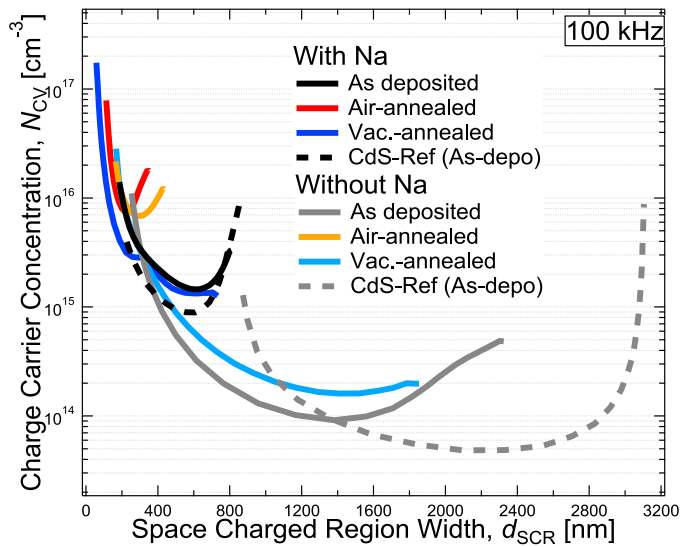


Fig. 8. N_{CV} -profiles of the GaO_x -buffered CIGSe solar cells with and without Na before and after thermal stress at 300°C for 20 min in air and under vacuum.

devices primarily causes a reduced FF , signifying a strong voltage dependent current loss. Unlike the effect of air-annealing, no notable changes in N_{CV} after vacuum-annealing are observed in both cases with and without Na. Moreover, strong kink and cross-over anomalies are evident in the JV -characteristics. The cross-over anomaly is defined as a crossing of dark and illuminated JV -curves at high forward bias [16]. This is likely to occur due to the presence of a back contact barrier [34]. In terms of the kink anomaly, as already mentioned above related to the CdS-buffer, several origins are possible. It could arise from an increased barrier for the photocurrent at the CIGSe/ GaO_x heterointerface [11], the formation of a p^+ layer on top of the CIGSe absorber leading to a narrower space charge region [35], a high acceptor defect density at the CIGSe/ GaO_x interface [8],

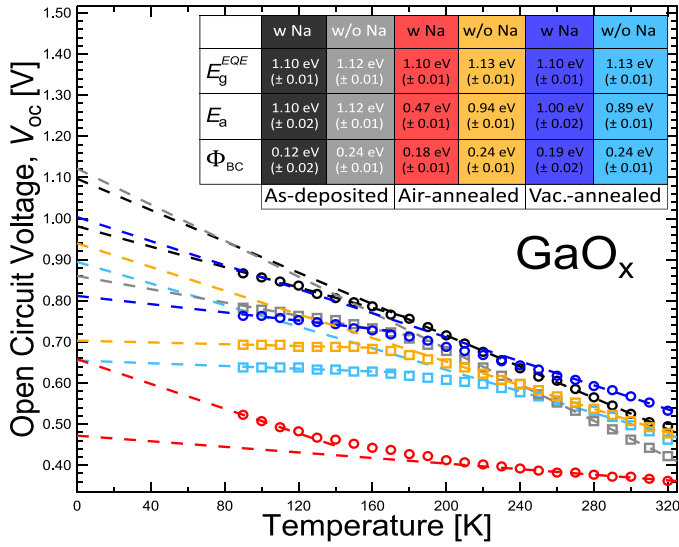
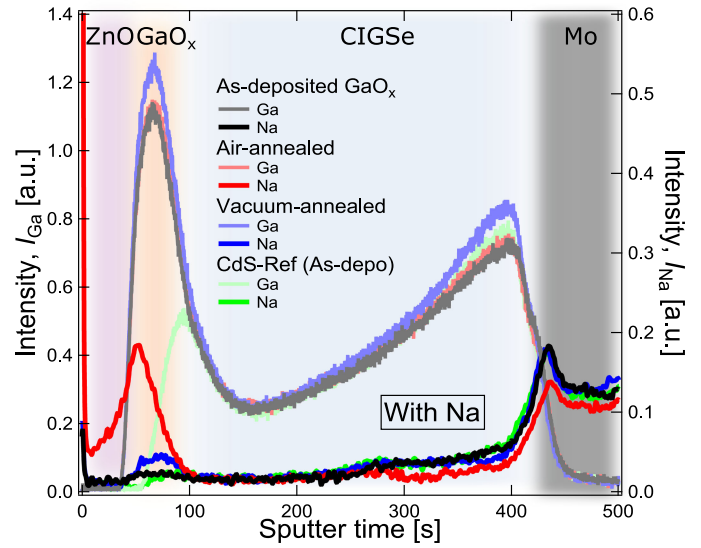


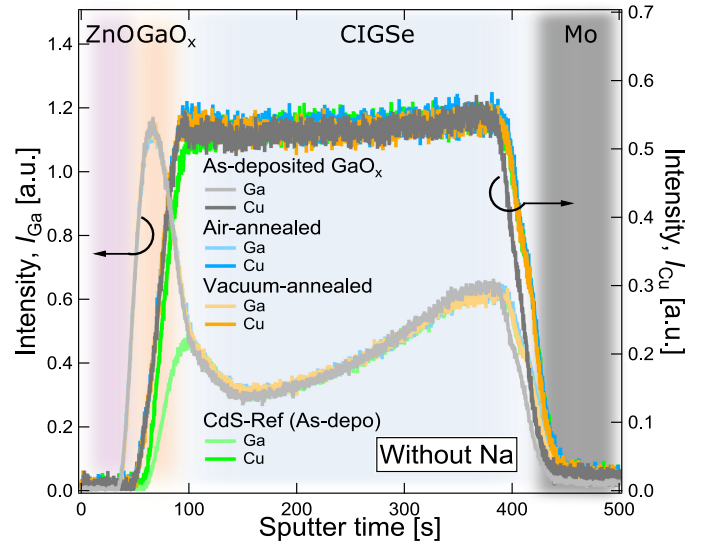
Fig. 9. V_{OC} - T characteristics under one sun illumination at temperatures from 90 to 320 K for the GaO_x -buffered-CIGSe solar cells with (circles) and without Na (squares).

which leads to Fermi level pinning at the CIGSe/ GaO_x heterojunction, acceptor defects in the GaO_x layer itself [8], [36] or a combination of these.

The V_{OC} - T characteristics extracted from JV - T measurements and GD-OES in-depth profiles of the respective devices help to reveal the causes underlying these anomalies. Fig. 9 hence suggests that the main recombination mechanisms of the as-deposited devices with and without Na lies within the space charge region, similar to the case of the as-deposited CdS-buffered device with Na shown in Fig. 3. Interestingly, the higher E_a of the as-deposited GaO_x -buffered device without Na compared with the CdS reference without Na could originate from the air-annealing of the absorber layer before the GaO_x deposition due to the beneficial effect of air-annealing of bare CIGSe absorber on the main recombination and V_{OC} , which we reported previously [7]. Notwithstanding, in case of $E_a \approx E_g$ solar cell devices can still be limited at the interface [37]. This could be the reason for the inherent low V_{OC} of the as-deposited GaO_x devices, when compared with the CdS counterparts. As expected, comparable Φ_{BC} for as-deposited devices with and without Na are observed due to the effect of the Na-presence at the CIGSe/Mo interface as in the case of as-deposited CdS-buffered devices with and without Na. Annealing of the GaO_x -buffered devices, regardless of the environment and Na-presence, gives rise to $E_a < E_g$ despite the fact that annealing of these devices seems to be able to increase their V_{OC} . These results signify that the recombination at the GaO_x /CIGSe interface should be enhanced. That is to say, another effect of the annealing is reflected in an increased Φ_{BC} for the devices with Na. Having said that, Φ_{BC} of the devices without Na were not affected further by annealing as was the case for CdS-buffered devices without Na. The behavior of the air-annealed device with Na at low temperatures shows an increase in V_{OC} instead of a voltage saturation, which would be expected, even though



(a)



(b)

Fig. 10. Unquantified Ga, Cu, and Na in-depth profiles of as-deposited and air-annealed GaO_x -buffered samples.

similar measurements have been performed on this sample. This puzzling behavior could not yet be understood.

Fig. 10(a) and (b) show the unquantified Ga and Na (for devices with Na) as well as Ga and Cu (for devices without Na) in-depth profiles of the as-deposited and annealed GaO_x -buffered solar cells along with their CdS-reference devices. Even though all samples show almost identical Ga profiles, a strong Na out-diffusion from and throughout the CIGSe absorber layer into the ZnO and GaO_x layers is apparent after air-annealing [see Fig. 10(a)], while a slight increment of Na-intensity is exclusively observed within the GaO_x and at the GaO_x /CIGSe interface after vacuum-annealing. As for the GaO_x -buffered devices without Na, there is the possibility of Cu diffusing toward the front contact layer in absence of Na. To illustrate this, Cu in-depth profiles together with Ga-profiles are shown

in Fig. 10(b). It is worth to note that all the profiles are aligned according to the Ga-onset except for the CdS-reference, that is aligned at the notch of the Ga-profile of the as-deposited GaO_x sample. There are no observable changes in both Ga and Cu profiles.

Since there is no Na-accumulation near the CIGSe surface region after thermal exposure in any case, this suggests that no p^+ -layer is formed on top of the CIGSe and can therefore be ruled out as a cause for a kink anomaly. In regard to the Na out-diffusion from the CIGSe absorber, the amount of Na decreases at the CIGSe/Mo interface after annealing and in an even more pronounced way for the air-annealed device. This again confirms the observed increases in Φ_{BC} stated above. Furthermore, Na-diffusion into the AZO layer after air-annealing intensifies the degeneration of the AZO-conductivity (956 Ω/sq) by Na-diffusion through the GaO_x layer, while air-annealing of the device without Na exhibit much lower sheet resistance (344 Ω/sq), similar to the cases observed in CdS-buffered devices. Accordingly, the series resistance of these devices is high, which explains to some extent the drop in J_{SC} of the air-annealed GaO_x-buffered devices.

Kim *et al.* have shown using high energy X-ray photoelectron spectroscopy (HAXPES) that excess oxygen during the amorphous GaO_x deposition induced the removal of oxygen vacancy related subgap defects [38]. Likewise, Valenta *et al.* have shown that air-annealing of GaO_x layers on CIGSe leads to a passivation of subgap defects, while only a subtle modification of subgap defects is evident after vacuum-annealing compared with as-deposited layers [39]. This means that air-annealing leads to the passivation of the oxygen vacancy related subgap defects in the GaO_x layers, presumably indicating that thermionic emission is the dominant transport mechanism at the GaO_x/CIGSe interface. This holds for air-annealing of the devices with and without Na. However, annealing-induced Na-diffusion into the GaO_x [see Fig. 10(a)] creates acceptor like defects as proposed by [36]. This applies to the annealing of the Na-containing GaO_x-buffered devices. The magnitude of the acceptor defects located in GaO_x layer is much higher for the air-annealed device than for the vacuum-annealed device with Na.

Annealing induced Na-diffusion might be responsible for an increased number of Na-induced acceptor states at the CIGSe/GaO_x heterointerface and in the GaO_x layer itself, in particular for the air-annealed device with Na. The strong decrease in J_{SC} seen in the air-annealed devices with and without Na can be well correlated with a change of the transport mechanism (passivation of the subgap defects by air-annealing) at the interface and/or a severely reduced d_{SCR} induced by Fermi level pinning at the interface. Furthermore, similar to the CdS-buffered devices, an increased Φ_{BC} after annealing of the devices with Na as a consequence of Na-depletion at the CIGSe/Mo interface region and already existing high Φ_{BC} in the devices without Na explains the appearance of a cross-over anomaly in the JV -characteristics of the annealed GaO_x-buffered devices as also suggested by [34]. On the other hand, annealing of the devices, in general, results in inferior junction properties, which indicates a high defect density in the vicinity of the heterojunction, as rendered by the $V_{OC}-T$ in Fig. 9. As to

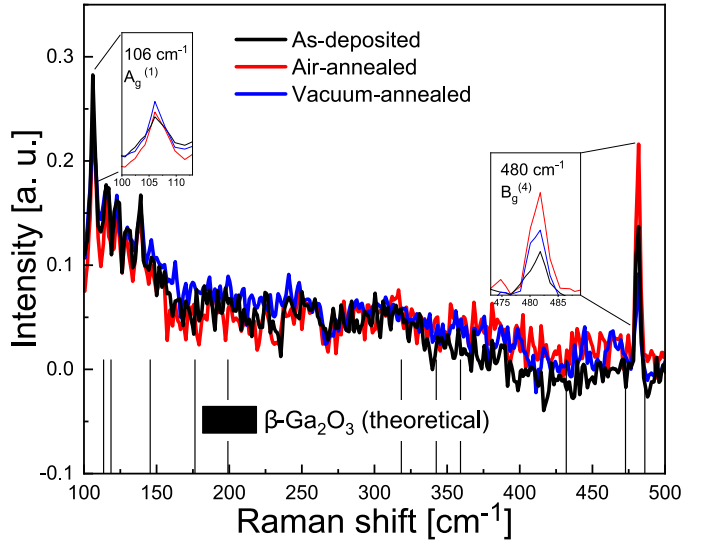


Fig. 11. Complementary structural analysis of the GaO_x thin films deposited on quartz before and after annealing treatment via Raman.

the stability of the vacuum-annealed devices with and without Na, their degradations are slowed down due to the fact that the vacuum-environment and the properties of GaO_x do not attract much mobile Na-ions and beneficial subgap defects in the GaO_x layers are not removed by vacuum-annealing [39], [40]. However, a high density of defects at the heterointerface present an impediment for all the devices.

D. Complementary Structural Analysis by Raman Measurement

Overall, passivation of the subgap defects in GaO_x layers and Na-migration in the GaO_x-buffered CIGSe devices are major problems. It seems that on the one hand, subgap defects facilitating current transport are rather prone to air-annealing. On the other hand, the GaO_x layers cannot hinder the Na-diffusion from the CIGSe absorber and prevent the attraction of mobile Na-ions toward the front contact layer. This raises the concern whether the sputter-deposited GaO_x layers are indeed entirely amorphous or possibly nanocrystalline and whether they conformally cover the whole surface of the CIGSe absorber, even though they seem to be amorphous according to the XRD-results in Fig. 6. To that end, we have employed Raman measurements on the GaO_x layers in order to conclusively confirm the structure of GaO_x. Fig. 11 demonstrates the Raman spectra of the as-deposited and annealed GaO_x thin films deposited on quartz glass. Surprisingly, all the samples show obvious Raman peaks attributed to the crystalline modes, even for the as-deposited sample indeed indicating a nanocrystalline growth of the GaO_x on CIGSe. The shifts, that are observed compared with β -Ga₂O₃ reference [41], are related to internal stresses in the nanocrystals. Both looking at the results from XRD and Raman together and due to the low intensity of the peaks, it can be deduced that the sputter deposited GaO_x layers as used in this work seem to contain nanocrystalline structures. This explains why the Na-diffusion is still a major challenge.

IV. CONCLUSION

Annealing of CdS-buffered CIGSe solar cells, independent of the annealing atmosphere, leads to severe degradation of the solar cell parameters. Na out-diffusion induces several problems such as an increased height of the back contact barrier, a decreased absorber charge carrier concentration, a reduction of the CIGSe/CdS junction quality (high interface recombination), acceptor trap states in the CdS layer by Na-presence and an increased series resistance due to a reduced conductivity of the AZO layer. Beside this, Cd-diffusion into the CIGSe absorber has been observed, presumably leading to the formation of an *n*-type surface on top of the CIGSe absorber layer. It was postulated that the wet nature of the CdS buffer layer in CIGSe solar cells facilitates the movement of mobile Na-ions leading to overall low PV-performances.

Considerable progress has been made regarding the employment of GaO_x as a buffer layer in terms of the thermal stability under vacuum, even though degradation of the PV-performances of the air-annealed GaO_x-buffered CIGSe devices is still similarly severe, but also, showing different degradation mechanisms. Air-annealing has induced a severe loss in *J*_{SC} possibly revealing the formation of a high barrier for the photocurrent at the CIGSe/GaO_x heterointerface by the passivation of beneficial oxygen vacancy-related subgap defects, Fermi level pinning at the interface and in the GaO_x due to a high density of acceptor defects and an increased series resistance due to a reduced conductivity of the AZO layer. Despite the fact that annealing of the GaO_x-buffered devices induces higher *V*_{OC}, interface recombination strongly prevails after annealing, indicating the sensitivity of the GaO_x/CIGSe interface to thermal annealing. Furthermore, Na-diffusion from the CIGSe absorber layer into the front contact layers is evident after annealing, even though the deposited GaO_x layers exhibit an amorphous structure according to XRD-results. Raman measurement, however, revealed the nanocrystalline structure of the GaO_x. All in all, the nanocrystalline structure of GaO_x can be seen as a hurdle toward thermal stability. Future work needs to be performed to elucidate whether undoubtedly an amorphous GaO_x as a buffer layer can help to achieve thermally stable CIGSe solar cells and whether the observed beneficial effect of the oxygen vacancy-related subgap defects in GaO_x presents an impediment toward thermal stability. Employing ultra thin amorphous GaO_x at the interface might be an alternative option toward thermal stability along with the possibility of passivating the critical interface to the CIGSe absorber. Alternative methods such as atomic layer deposition may be a viable step in the further development for a thermally stable CIGSe thin film solar device with GaO_x remaining a reasonable material choice.

ACKNOWLEDGMENT

The authors would like to thank B. Bunn, K. Mayer-Stillrich, J. Lauche, T. Münchenberg, S. Stutzke, M. Kirsch, and I. Dorbandt for technical support with respect to device fabrication and S. Stutzke, D. Schewitz, Z. Salami, S. Ghaderi, S. Knoop, and R. Gunder for support with device characterization. Colleagues from TU Berlin sincerely thank M. R. Wagner (Institute of Solid

State Physics) for making professional Raman measurements available.

REFERENCES

- [1] M. Nakamura *et al.*, "Cd-free Cu(In,Ga)(Se,S)₂ thin-film solar cell with record efficiency of 23.35%," *IEEE J. Photovolt.*, vol. 9, no. 6, pp. 1863–1867, Nov. 2019.
- [2] W. Shockley and H. J. Queisser, "Detailed balance limit of efficiency of p-n junction solar cells," *J. Appl. Phys.*, vol. 32, pp. 510–519, 1961.
- [3] S. P. Bremner, M. Y. Levy, and C. B. Honsberg, "Analysis of tandem solar cell efficiencies under AM1.5G spectrum using a rapid flux calculation method," *Progress Photovolt., Res. Appl.*, vol. 16, no. 3, pp. 225–233, 2008.
- [4] NREL, Golden, CO, USA, 2020, [Online]. Available: <https://www.nrel.gov/pv/cell-efficiency.html>
- [5] S. Kijima and T. Nakada, "High-temperature degradation mechanism of Cu(In,Ga)Se₂-based thin film solar cells," *Appl. Phys. Express*, vol. 1, 2008, Art. no. 075002.
- [6] L. L. Kazmerski, O. Jamjoum, and P. J. Ireland, "Formation, growth, and stability of the CdS/CuInSe₂ interface," *J. Vacuum Sci. Technol.*, vol. 21, pp. 486–490, 1982.
- [7] H. A. Yetkin *et al.*, "Decay mechanisms in CBD-CdS-Buffered Cu(In,Ga)Se₂ thin film solar cells after exposure to thermal stress - Understanding the role of Na," submitted to, *Photovoltaics: Research and Applications*. Hoboken, NJ, USA: Wiley, 2020.
- [8] M. D. Heinemann *et al.*, "Amorphous oxides as electron transport layers in Cu(In,Ga)Se₂ superstrate devices," *Physica Status Solidi (a)*, vol. 214, 2017, Art. no. 1600870.
- [9] M. Mohamed, K. Irmscher, C. Janowitz, Z. Galazka, R. Manzke, and R. Fornari, "Schottky barrier height of Au on the transparent semiconducting oxide β-Ga₂O₃," *Appl. Phys. Lett.*, vol. 101, 2012, Art. no. 132106.
- [10] H. A. Yetkin *et al.*, "Amorphous GaO_x and Its alloying for use as electron transport layer in CIGSe solar cells," in *Proc. 29th Int. Photovolt. Sci. Eng. Conf.*, Xi'an, China, submitted for publication.
- [11] M. D. Heinemann, J. Berry, G. Teeter, T. Unold, and D. Ginley, "Oxygen deficiency and Sn doping of amorphous Ga₂O₃," *Appl. Phys. Lett.*, vol. 108, 2016, Art. no. 022107.
- [12] H. A. Yetkin *et al.*, "Comparison of the thermal stability of differently buffered CIGSe solar cells," in *Proc. 47th IEEE Photovolt. Specialist Conf.*, 2020, pp. 1192–1197.
- [13] M. D. Heinemann *et al.*, "Evolution of opto-electronic properties during film formation of complex semiconductors," *Sci. Reports*, vol. 7, 2017, Art. no. 45463.
- [14] T. Kodalle *et al.*, "Glow discharge optical emission spectrometry for quantitative depth profiling of CIGS thin-films," *J. Analytic At. Spectrometry*, vol. 34, pp. 1233–1241, 2019.
- [15] A. Pflug, V. Sittinger, F. Ruske, B. Szyszka, and G. Dittmar, "Optical characterization of aluminum-doped zinc oxide films by advanced dispersion theories," *Thin Solid Films*, vol. 455/456, pp. 201–206, 2004.
- [16] R. Scheer, and H. W. Schock, *Chalcogenide Photovoltaics: Physics, Technologies, and Thin Film Devices*. Hoboken, NJ, USA: Wiley, 2011.
- [17] T. Ott *et al.*, "Verification of phototransistor model for Cu(In,Ga)Se₂ solar cells," *Thin Solid Films*, vol. 582, pp. 392–396, 2015.
- [18] T. Nakada, M. Mizutani, "Improved efficiency of Cu(In,Ga)Se₂ thin film solar cells with chemically deposited ZNS buffer layers by air-annealing-formation of homojunction by solid phase diffusion," in *Proc. 28th IEEE Photovolt. Specialist Conf.*, 2000, pp. 529–534.
- [19] C. Persson, Y. Zhao, S. Lany, A. Zunger, "n-type doping of CuInSe₂ and CuGaSe₂," *Phys. Rev. B.*, vol. 72, 2005, Art. no. 035211.
- [20] W. Gordy, "Electronegativities of the elements," *J. Chem. Phys.*, vol. 24, pp. 439–444, 1956.
- [21] A. Kylner, A. Rockett, L. Stolt, "Oxygen in solution grown CdS films for thin film solar cells," *Solid State Phenomena*, vol. 51, pp. 553–540, 1996.
- [22] R. Caballero *et al.*, "Influence of Na on Cu(In,Ga)Se₂ solar cells grown polyimide substrates at low temperature: Impact Cu(In,Ga)Se₂/Mo interface," *Appl. Physics Lett.*, vol. 96, 2010, Art. no. 092104.
- [23] R. Caballero *et al.*, "Impact of Na on MoSe₂ formation at the CIGSe/Mo interface in thin-film solar cells on polyimide foil at low process temperatures," *Acta Materialia*, vol. 63, pp. 54–62, 2014.
- [24] A. Rothwarf, "CdS/Cu₂S solar cell: Basic operation and anomalous effects," *Solar Cells*, vol. 2, pp. 115–140, 1980.
- [25] A. O. Pudov, J. R. Sites, M. A. Contreras, T. Nakada, and H. W. Schock, "CIGS JV-distortion in the absence of blue photons," *Thin Solid Films*, vol. 480, pp. 273–278, 2005.

- [26] A. Rockett, J. K. J. van Duren, A. Pudov, and W. N. Shafarman, "First quadrant phototransistor behavior in CuInSe₂ photovoltaics," *Sol. Energy Materials Solar Cells*, vol. 118, pp. 141–148, 2013.
- [27] D. Ledinek, O. Donzel-Gargand, M. Sköld, J. Keller, and M. Edoff, "Effect of different Na supply methods on thin Cu(In,Ga)Se₂ solar cells with Al₂O₃ rear passivation layers," *Sol. Energy Mater. Sol. Cells*, vol. 187, pp. 160–169, 2018.
- [28] J. B. Varley, V. Lordi, X. He, and A. Rockett, "First principles calculations of point defect diffusion in CdS buffer layers: Implications for Cu(In,Ga)(Se,S)₂ and Cu₂(Zn,Sn)(Se,S)₄-based thin-film photovoltaics," *J. Appl. Physics*, vol. 119, 2016, Art. no. 025703.
- [29] B. K. Meyer, J. Sann, and A. Zeuner, "Lithium and sodium acceptors in ZnO," *Superlattices Microstructures*, vol. 38, pp. 344–348, 2005.
- [30] B. K. Meyer *et al.*, "On the role of group I. elements in ZnO," *Appl. Phys. A.*, vol. 88, pp. 119–123, 2007.
- [31] R. A. Street, *Technology and application of Amorphous Silicon*, Berlin, Germany: Springer, vol. 37, 2000.
- [32] F. Urbach, "Long-wavelength edge of photographic sensitivity and of the electronic absorption of solids," *Physical Rev.* vol. 92-5, 1953, Art. no. 1324.
- [33] T. Koida, Y. Kamikawa-Shimizu, A. Yamada, H. Shibata, and S. Niki, "Cu(In,Ga)Se₂ solar cells with amorphous oxide semiconducting buffer layers," *IEEE J. Photovolt.*, vol. 5, pp. 956–961, May 2015.
- [34] A. Niemegeers, and M. Burgelman, "Effects of the Au/CdTe back contact on IV and CV characteristics of Au/CdTe/CdS/TCO solar cells," *J. Appl. Phys.*, vol. 81, pp. 2881–2886, 1997.
- [35] M. Nichterwitz, R. Caballero, C. A. Kaufmann, H. W. Schock, and T. Unold, "Generation-dependent charge carrier transport in Cu (in, ga) Se₂/CdS/ZnO thin-film solar-cells," *J. Appl. Phys.*, vol. 113, 2013, Art. no. 0 44515.
- [36] M. D. Heinemann *et al.*, "Cu(In,Ga)Se₂ superstrate solar cells: Prospects and limitations," *Progress Photovoltaics: Res. Appl.*, vol. 23, pp. 1228–1237, 2015.
- [37] R. Scheer, "Activation energy of heterojunction diode currents in the limit of interface recombination," *J. Appl. Phys.*, vol. 105, 2009, Art. no. 104505.
- [38] J. Kim *et al.*, "Conversion of an ultra-wide bandgap amorphous oxide insulator to a semiconductor," *NPG Asia Mater.*, vol. 9, no. 3, pp. e 359–e359.
- [39] D. Valenta *et al.*, "Annealing induced intermixing and passivation of the front contact in Cu(In,Ga)Se₂ devices—A spectroscopic view on CdS and GaO_x," Talk Presented at Virtual Chalcogenide PV Conf., 2020.
- [40] L. Dong, R. Jia, B. Xin, B. Peng, and Y. Zhang, "Effects of oxygen vacancies on the structural and optical properties of β-Ga₂O₃," *Sci. Reports*, vol. 7, pp. 1–12, 2017.
- [41] C. Kranert, C. Sturm, R. Schmidt-Grund, and M. Grundmann, "Raman tensor elements of β-Ga₂O₃," *Sci. Reports*, vol. 6, 2016, Art. no. 35964.